

## Two-dimensional and three-dimensional vortex lattice dynamics in $\text{DyBa}_2\text{Cu}_3\text{O}_7-(\text{Y}_{1-x}\text{Pr}_x)\text{Ba}_2\text{Cu}_3\text{O}_7$ coupled heterostructures

J.-M. Triscone, P. Fivat, M. Andersson, M. Decroux, and Ø. Fischer

*Département de Physique de la Matière Condensée, University of Geneva, 24 Quai E.-Ansermet, 1211 Geneva 4, Switzerland*

(Received 20 December 1993)

Vortex dynamics is studied in coupled multilayer structures, containing  $N$  24-Å-thick  $\text{DyBa}_2\text{Cu}_3\text{O}_7$  layers, each separated from the next by 96 Å of  $(\text{Y}_{1-x}\text{Pr}_x)\text{Ba}_2\text{Cu}_3\text{O}_7$  ( $x=0.4, 0.55$ ). When the magnetic field is parallel to the  $c$  axis, we find that the activation energy  $U$  for flux motion increases linearly with the number of superconducting layers  $N$  in the structure for  $N < 3$ . This linear increase is the result of the coupled motion of pancake vortices belonging to different  $\text{DyBa}_2\text{Cu}_3\text{O}_7$  layers. For larger  $N$  samples the activation energy saturates meaning that the vortex lattice is turning three dimensional. In contrast to samples whose vortex lattice is purely two dimensional and for which we find the activation energy for flux motion proportional to  $\log_{10}B$ , samples in these series show a crossover to a power-law behavior,  $U \approx B^{-0.5}$ , at a magnetic field  $H^*$  which decreases as  $N$  increases.

### I. INTRODUCTION

The  $H$ - $T$  phase diagram of high- $T_c$  superconductors is one of the most fascinating and discussed aspects of these materials. Questions related to, for instance, thermal fluctuations, the irreversibility line, or the existence of a vortex glass and/or a melting transition are still under debate.<sup>1</sup> For several of these problems the dimensionality of the vortex lattice is a crucial parameter and predictions concerning the low-temperature phase of the vortex lattice have been made depending on its dimensionality.<sup>2</sup> High- $T_c$  superlattices may be a useful tool to address some of these questions. The main advantage of these artificial structures is to provide a way to control and modify the vortex lattice parameters and, in particular, its dimensionality, allowing to track the effects of such changes on specific physical properties. Recently,<sup>3-5</sup> we studied extensively the flux dynamics in  $\text{YBa}_2\text{Cu}_3\text{O}_7/\text{PrBa}_2\text{Cu}_3\text{O}_7$  (YBCO/PrBCO) superlattices. In these superlattices the thickness of "insulating" PrBCO, 96 Å, is sufficient to essentially decouple the superconducting layers (as will be discussed below, magnetic coupling is irrelevant to this study). The main result was that the activation energy for flux motion  $U$ , in the regime of linear  $I$ - $V$  characteristics, is proportional to the YBCO thickness in the multilayers for  $d$ -YBCO  $< 300$  Å, and has a logarithmic field dependence, for  $H$  parallel to the  $c$  axis. The scaling of the activation energy with the YBCO thickness reflects the absence of interaction between pancake vortices of different superconducting layers. The correlation length  $L_c$  involved in this activated motion of vortices is found to be about 400 Å implying a two-dimensional (2D) vortex lattice in YBCO layers thinner than 400 Å. The logarithmic field dependence of the activation energy found in YBCO/PrBCO multilayers as well as in thin YBCO layers<sup>6</sup> has its origin in the 2D nature of the vortex lattice as discussed below. Notice here that the correlation length  $L_c$ , as defined and measured in this work is not identical to the Larkin-Ovchinnikov collective pinning correlation length,<sup>7</sup> although certainly related to it. Ongoing measurements of

creep at low temperature<sup>8</sup> give a somewhat lower value for  $L_c$ .

In this paper we report on a study of vortex dynamics in structures where proximity effect coupling is introduced between the superconducting layers by replacing the insulating PrBCO by an  $(\text{Y}_{1-x}\text{Pr}_x)\text{BCO}$  alloy. The idea is to generate a coupling or a partial coupling of the pancake vortices belonging to different superconducting layers. When the superconducting layer thickness  $d_s$  is chosen much smaller than the  $L_c$  of bulk YBCO, each layer behaves as a 2D sheet containing pancake vortices. Coupling pancakes of different layers should result in a larger effective thickness and thus in a marked change of the activation energy. This coupling will produce a correlated motion of vortices over a characteristic number of layers  $N_c$  above which shear of the vortex structures becomes important. Preliminary reports of this work can be found in Refs. 9 and 10.

### II. STRUCTURE OF THE SAMPLES

To test these ideas we prepared series of samples where the number of superconducting layers was systematically varied. All the samples contain 24-Å-thick  $\text{DyBa}_2\text{Cu}_3\text{O}_7$  (DyBCO) layers separated by 96 Å of  $(\text{Y}_{1-x}\text{Pr}_x)\text{BCO}$ ,  $x=0.4, 0.55$ , and 1.0.  $(\text{Y}_{1-x}\text{Pr}_x)\text{BCO}$  alloys have been successfully used in superconductor-normal-metal-superconductor junctions<sup>11</sup> and, in superlattices, for studying the  $T_c$  of ultrathin layers<sup>12</sup> as well as the behavior of the critical current in presence of coupling.<sup>13</sup> These alloys have the advantage that the conductivity and the critical temperature are controlled by the amount of yttrium in the alloy.<sup>14</sup> Before growing the heterostructures we investigated the transport properties of single-alloy thin films.<sup>10</sup>  $(\text{Y}_{0.6}\text{Pr}_{0.4})\text{BCO}$  films have a metallic behavior of the resistivity, with a resistivity ratio  $\rho(300\text{ K})/\rho(100\text{ K})$  of 1.4, a room-temperature resistivity of  $\approx 1000\ \mu\Omega\text{ cm}$ , and a  $T_c(90\%)$  of 43.6 K. The  $(\text{Y}_{0.45}\text{Pr}_{0.55})\text{BCO}$  films display a semi-conducting-like behavior of the resistivity with a room-temperature value of about  $1200\ \mu\Omega\text{ cm}$ , and  $\rho(300\text{ K})/\rho(100\text{ K})=0.9$ . Fi-

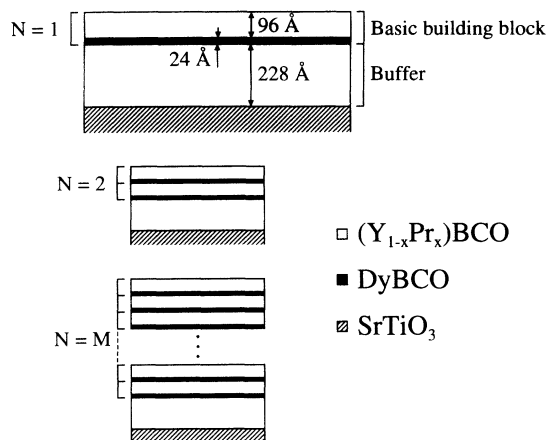


FIG. 1. Schematic diagram of the samples. Each sample consists of an  $\approx 230$ -Å-thick  $(Y_{1-x}Pr_x)BCO$  buffer layer upon which a basic building block of 24 Å-DyBCO-96 Å- $(Y_{1-x}Pr_x)BCO$  is deposited  $N$  times. Illustrated are the  $N=1$ ,  $N=2$ , and  $N=M$  sequences.

nally, the pure PrBCO thin films, prepared with the conditions described below, are characterized by a room-temperature resistivity of about  $10^4$ – $10^5$   $\mu\Omega$  cm,  $\rho(300\text{ K})/\rho(100\text{ K}) \approx 0.01$  and a large low-temperature resistivity,  $\approx 10^8$   $\mu\Omega$  cm at 50 K (a typical temperature for our measurements).

The series are built as illustrated in Fig. 1. Each sample has an  $\approx 230$  Å  $(Y_{1-x}Pr_x)BCO$  buffer layer. On top, a basic building block, 24 Å-DyBCO-96 Å- $(Y_{1-x}Pr_x)BCO$  is deposited  $N$  times, with  $N$  between 1 and 15. The samples are dc sputtered in a mixture of Ar and  $O_2$  ( $Ar + O_2 = 635$  mTorr, 10%  $O_2$ ) onto (100)  $SrTiO_3$  substrates heated to 750 °C. More details on the preparation as well as on the properties of the alloys can be found in Refs. 10 and 15.

### III. CHARACTERIZATION AND CALIBRATIONS

X-ray-diffraction is a powerful tool for characterizing thin films as well as for deposition rate calibrations. For superlattices the signature of the artificial modulation is the presence in the  $\theta$ - $2\theta$  x-ray diffractograms of satellite peaks.<sup>16</sup> For thin samples (typically several hundreds of Å) additional peaks also appear around the main reflections due to finite-size effects. A very spectacular example of finite-size effects, observed for a  $GdBa_2Cu_3O_7$  thin film, can be found in Ref. 17.

Figures 2 and 3 are  $\theta$ - $2\theta$  x-ray diffractograms of thin PrBCO and DyBCO samples around the (001) reflection. The finite-size related peaks, indexed  $\pm j$ , can be used both to measure precisely the average thickness, with an accuracy of 5–10 %, and to estimate the roughness of the films, as will be described in a forthcoming publication.<sup>18</sup> The dashed lines drawn in Figs. 2 and 3 are calculations of the x-ray spectrum assuming perfect crystalline coherence throughout the films, without any surface roughness. The theoretical x-ray spectrum is given by:<sup>18</sup>

$$I(\theta) \propto \left[ \frac{\sin(\pi n c \sin\theta/\lambda_x)}{\sin(\pi c \sin\theta/\lambda_x)} \right]^2,$$

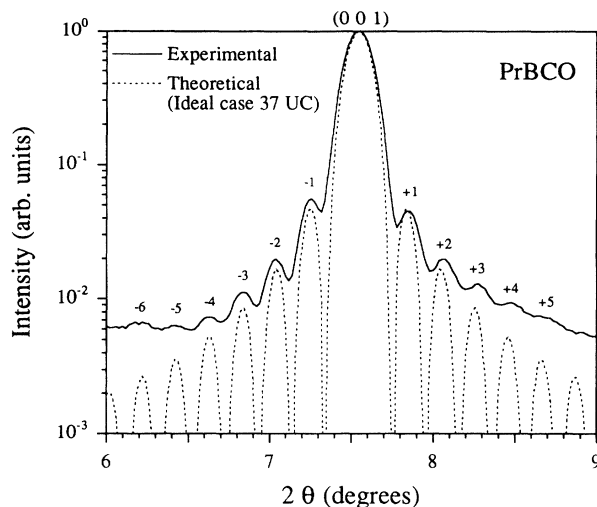


FIG. 2.  $\theta$ - $2\theta$  x-ray diffractogram around the (001) reflection of a thin PrBCO sample. The  $\pm j$  indexed additional peaks are due to finite-size effects. The dashed line is a fit to the experimental spectrum as discussed in the text. The average thickness is found to be about 37 unit cells, i.e.,  $\approx 433$  Å.

where  $c$  is the lattice parameter parallel to the normal surface,  $\lambda_x$  is the x-ray wavelength (1.542 Å for  $Cu K_\alpha$ ), and  $n$  is the thickness in unit cells. From the fits in Figs. 2 and 3 one can estimate the average thickness to be about 37 unit cells and 15 unit cells for the PrBCO and DyBCO layers, respectively. This method of measuring the thickness gives systematically an average value of one or two unit cells less than the thickness forecast from rate calibrations determined by satellite peak analysis in multilayers. This difference is possibly related to a poorer crystallization of the first and last unit cells of the layer. The position of the first peak around the (001) reflection is almost insensitive to roughness.<sup>18</sup> The large number of

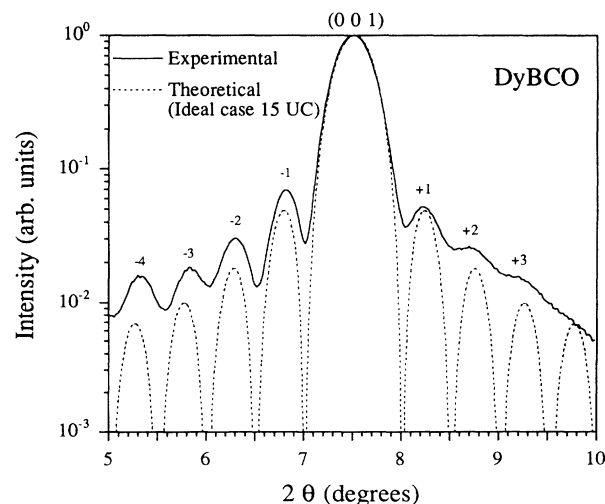


FIG. 3.  $\theta$ - $2\theta$  x-ray diffractogram around the (001) reflection of a thin DyBCO sample. The dashed line is a fit to the experimental spectrum as discussed in the text. The average thickness is found to be about 15 unit cells, i.e.,  $\approx 175.5$  Å.

secondary peaks in the figures is a sign that the films investigated are relatively smooth. This fact is of course important for heterostructure growth in general. Quantitative analysis of the film roughness and correlation with scanning tunnel microscope studies will be reported elsewhere.<sup>18</sup>

#### IV. STUDY OF THE VORTEX DYNAMICS

To probe vortex dynamics, we measured the activation energies for flux motion in fields parallel and perpendicular to the  $ab$  plane, in the region close to  $T_c$  where the  $I$ - $V$  characteristics are linear. The activation energies are obtained from a measure of the resistivity  $\rho$  as a function of temperature and magnetic field using standard four points measurements. When  $\rho(T)$  is plotted in an Arrhenius way, i.e.,  $\ln\rho$  vs  $1/T$ , the activated character of the resistivity becomes apparent. Figure 4 shows Arrhenius plots of the resistivity for the  $N=1$  and  $N=2$  samples of the DyBCO-(Y<sub>0.6</sub>Pr<sub>0.4</sub>)BCO series. The activation energies  $\bar{U}$  are defined as the slope of the lower part [ $\rho < 0.01\rho(T_{c\text{onset}})$ ] of the Arrhenius plot. As discussed in Ref. 19, the temperature dependence of  $U$ , typically  $(1-T/T_c)^q$ , may complicate the interpretation of the data. When  $q=1$  the bottom part of the  $\ln(\rho)$  vs  $1/T$  curve is a true straight line whose slope is  $U(T=0)$ . If  $q > 1$  a curvature is visible on the bottom part of the curve. In this work we either rely on tracing a straight line on the bottom part of the  $\ln\rho$  vs  $1/T$  curve, whose slope is defined as  $\bar{U}$ , or we use the scaling technique described below, which partly avoids the curvature problem and allows us to compare the activation energies from sample to sample.

In Fig. 4 we find, within our precision, that  $\bar{U}(N=2)$  is exactly twice  $\bar{U}(N=1)$  for each magnetic field. In the

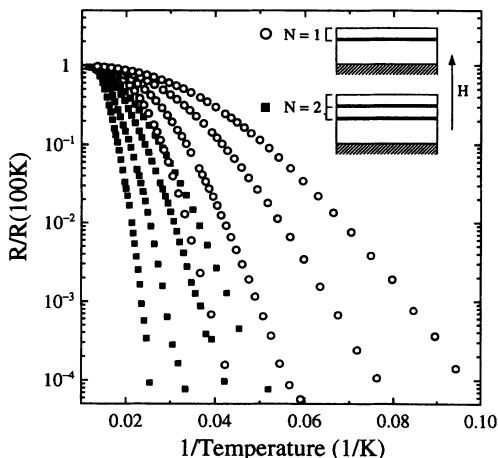


FIG. 4.  $R$  vs  $1/T$  for the  $N=1$  and  $N=2$  DyBCO-(Y<sub>0.6</sub>Pr<sub>0.4</sub>)BCO samples, and for magnetic fields of 1, 3, 6, and 9 T. Measuring the  $N=1$  and  $N=2$  slopes of the  $\ln\rho$  vs  $1/T$  curve [for  $\rho < 0.01\rho(T_{c\text{onset}})$ ] shows that  $\bar{U}(N=2, H) = 2\bar{U}(N=1, H)$ . The inset shows the structure of the  $N=1$  and  $N=2$  samples and the field configuration. The thick black lines are the 24-Å-thick DyBCO layers while the white regions are 230-, and 96-Å-thick (Y<sub>0.6</sub>Pr<sub>0.4</sub>)BCO, for the buffer and the separator layers, respectively.

DyBCO-(Y<sub>0.45</sub>Pr<sub>0.55</sub>)BCO series we find a very similar result;  $\bar{U}(N=2)$  is twice  $\bar{U}(N=1)$ , while in the DyBCO-PrBCO series we find within experimental fluctuations that  $\bar{U}$  is independent of  $N$  up to  $N=6$ . The factor of 2 observed in the structures containing the alloy instead of insulating PrBCO can be interpreted as follows: in the  $N=1$  sample the activation energy measured corresponds to the one of pancakes of thicknesses 24 Å (or more due to some proximity effect). In the  $N=2$  sample, due to the coupling, pancakes belonging to both layers are stacked and move together. Since the activation energy is proportional to the effective thickness involved in the flux jumps and each layer thickness is much smaller than  $L_c$ , we obtain  $\bar{U}(N=2) = 2\bar{U}(N=1)$  for strong enough coupling. As we discuss in Sec. VI the coupling responsible for the correlated motion of vortices has to come from proximity effect. The magnetic coupling of the pancake vortices cannot be the origin of this effect, simply because the correlated motion is not observed when insulating PrBCO is used instead of an alloy.

To better illustrate the factor of 2 between the activation energies of the  $N=1$  and  $N=2$  samples we used the data of Fig. 4 and multiplies the  $1/T$  scale of the  $N=1$  sample by a factor  $\frac{1}{2}$ . Since  $\ln(\rho) \approx -U(T) \cdot 1/T$ , multiplying the  $1/T$  scale of the  $N=1$  sample by  $\frac{1}{2}$  corresponds to an effective rescaling of  $U(N=1)$  by a factor of 2. To highlight the result we normalized the resistances, and shifted the transitions to account for the  $T_c$  difference. The result is shown in Fig. 5. The possible errors introduced by this technique are discussed below. As can be seen, the curves for each magnetic field fall on top of each other demonstrating the ratio of two between the activation energies of the  $N=1$  and  $N=2$  samples. Notice that the only important fact is that the slopes of the low  $\rho$  part,  $< 0.01\rho(T_{c\text{onset}})$ , are identical. The collapse of the points at higher temperatures is probably fortuitous and do not occur systematically for other scalings. The advantage of this scaling technique is that it allows us to superimpose the curves upon each other and to determine the ratio between the activation energies of two samples without having to make assumptions about the temperature dependence of  $U$ . However, one remaining problem with this technique is that we compare local slopes ( $\partial \ln\rho / \partial T$ ) at different reduced temperatures for different samples. By taking  $U(T) = U(T=0)(1-T/T_c)^q$  for the temperature dependence of  $U$  and defining  $\delta = q - 1$  and  $t = T/T_c$ , we made an estimate of the error introduced by the temperature dependence of  $U$  on the ratio  $R$  of the activation energies obtained by the rescaling. We find that the ratio between the local slopes ( $\partial \ln\rho / \partial T$ )<sub>T1</sub> and ( $\partial \ln\rho / \partial T$ )<sub>T2</sub> (taken at temperature  $T1$  for the  $N=1$  sample and at  $T2$  for the  $N=2$  sample) and the ratio of the zero-temperature activation energies  $U(N=1, T=0)/U(N=2, T=0)$  is

$$\frac{(\partial \ln\rho / \partial T)_{T1} / (\partial \ln\rho / \partial T)_{T2}}{U(N=1, T=0) / U(N=2, T=0)} = \frac{(1 + \delta t_1)(1 - t_1)^\delta}{(1 + \delta t_2)(1 - t_2)^\delta} \quad (1)$$

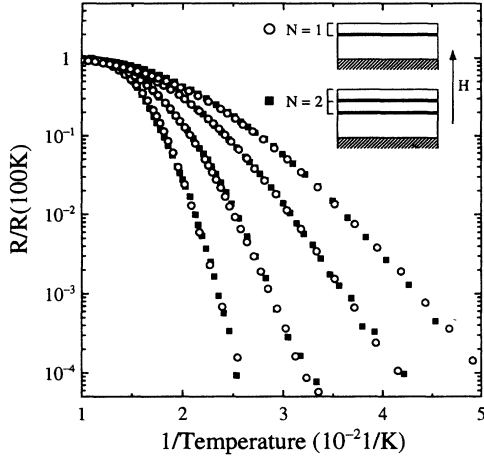


FIG. 5.  $R$  vs  $1/T$  for the  $N=1$  and  $N=2$  DyBCO- $(Y_{0.6}Pr_{0.4})$ BCO samples, and for magnetic fields of 1, 3, 6, and 9 T. The resistivities have been normalized and the  $1/T$  scale of the  $N=1$  sample has been multiplied by a factor of  $\frac{1}{2}$  to illustrate the ratio of two between the activation energies of the two samples. The inset shows the structure of the  $N=1$  and  $N=2$  samples and the field configuration. The thick black lines are the 24-Å-thick DyBCO layers while the white regions are 230-, and 96-Å-thick  $(Y_{0.6}Pr_{0.4})$ BCO, for the buffer and the separation layers, respectively.

By estimating the mean field  $T_c$  and taking  $q=1-1.5$  in the  $U(T)$  dependence, we find this ratio, depending on the  $T_c$  criteria and the field, to be 1 within an error of 5%. Since our experience shows that the direct estimate of  $\bar{U}$  or the use of the rescaling technique gives essentially the same result, the direct measure of  $\bar{U}$  will be used in the following [i.e., measuring the slope of the  $\ln\rho$  vs  $1/T$  curve for  $\rho < 0.01\rho(T_{c \text{ onset}})$ ].

Figure 6 shows a principal result of this study. Illustrated are the activation energies for flux motion  $\bar{U}$  as a function of  $N$ , the number of superconducting layers in the structure, for the three series of samples and in a magnetic field of 1 T parallel to the  $c$  axis. Similar graphs can be obtained for other magnetic fields.<sup>10</sup> The main point to note in Fig. 6 is the difference between the PrBCO series and the alloy series. For the former one the activation energies are rather constant within fluctuations up to  $N=6$ . For larger  $N$  an increase of the activation energies, also noticed in a preliminary study onto similarly built structures containing 36 Å-DyBCO layers, is observed, possibly attributed to a relaxation of the strains in the layers.<sup>20</sup> In sharp contrast to this behavior, the alloy series display a linear increase of the activation energies for  $N < 3-4$  followed by a progressive saturation. We interpret the linear increase as the result of the coupled motion of pancakes belonging to different layers. For  $N > 2-3$  the proportionality between  $\bar{U}$  and  $N$  is lost and the activation energy progressively saturates. From this graph one deduces that  $N_c$ , the critical number of layers above which “perfect” coupling is lost, is 2–3. Above  $N_c$  the shear of the vortex lattice becomes important and the vortices do not behave any more as rigid rods. This re-

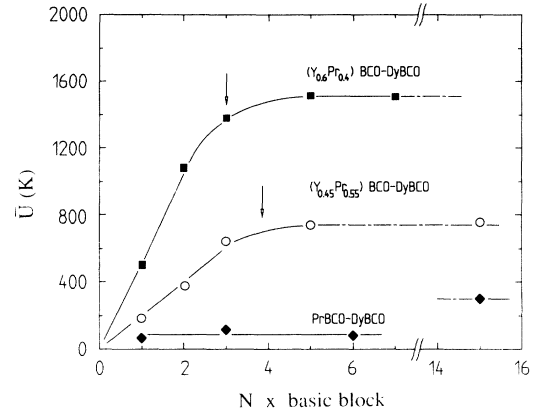


FIG. 6. DyBCO- $(Y_{1-x}Pr_x)$ BCO ( $x=0.4, 0.55,$  and 1) activation energies  $\bar{U}$  as a function of  $N$  and for a field of 1 T. For both alloy series the arrows indicate approximately  $L_c^*$  defined as the thickness at which the extrapolation of the linear increase of  $\bar{U}$  crosses the plateau value. The solid lines are guides to the eye.

sult also means that the vortex lattice dimensionality crosses over from 2D, where the vortices can be seen as perfectly rigid, to 3D where the vortices have a correlation length  $L_c^*$  smaller than the thickness of the sample, meaning that the vortex dynamics does not depend any more on the sample thickness (actually, as will be discussed below, details of the magnetic-field dependence of  $\bar{U}$  are still sensitive to the thickness). This system seems thus ideal to probe the effect of a change of the vortex lattice dimensionality on the physical properties.

The correlation lengths for these artificial structures, indicated by the arrows in Fig. 6 and defined as the thickness at which the extrapolation of the linear increase of  $\bar{U}$  crosses the plateau value, are  $\approx 360$  and  $\approx 480$  Å, for the  $x=0.4$ , and  $x=0.55$  series, respectively. These correlation lengths mean that about two or three stacked pancake vortices have a coupled motion in 24 Å-DyBCO/96 Å- $(Y_{0.6}Pr_{0.4})$ BCO superlattices while in the  $x=0.55$  series three to four pancakes are coupled. The larger value in the latter is, at first view, a surprising result since the coupling seems to be more important through the nonsuperconducting alloy. However, as can be seen in Fig. 6, the values of  $\bar{U}$  are different for a given  $N$  (lower in the 0.55 series than in the 0.4 series) meaning that the properties of thin DyBCO layers change as a function of  $x$  (this difference is related to the fact that superconductivity in ultrathin layers is strongly influenced by the environment as shown by other studies, see, for example, Ref. 12). Now, the smaller  $\bar{U}(N=1)$ , the smaller the energy necessary to couple pancakes in different layers [in first approximation the coupling energy  $J$  has to be of the order of  $\bar{U}(N=1)$  to be able to drag the vortices]. The larger  $L_c^*$  observed in the 0.45 series may thus be the result of the lower activation energy of a single pancake in this series. Another possibility is that the difference in  $L_c^*$  between the two series results from the particular nature of the coupling through the  $(Y_{0.45}Pr_{0.55})$ BCO alloy. This compound being close to the metal-insulator transi-

tion, the expected long localization length may allow a long distance proximity coupling.

Another point to notice is that, although the activation energies (the plateau values) of the alloy series are about 10–20 times smaller than in YBCO, the values obtained for  $L_c^*$  are close to the 400 Å obtained in pure YBCO.<sup>3</sup> It is not clear at present whether or not the similarity of the correlation length is fortuitous or whether it reflects some intrinsic property of the vortex lattice.

## V. TEST SAMPLES

As we mentioned just above the series of samples containing DyBCO and PrBCO display an abrupt increase of the activation energies which occurs above  $N=6$  for the DyBCO-PrBCO series discussed here, and at  $N=8$  for a similarly built series containing 36 Å of DyBCO.<sup>20</sup> It is only above the jump that we do find activation energy values comparable (within a factor of 2) to the ones obtained in YBCO/PrBCO multilayers studied in Ref. 3. We think that the observed jump may be related to the relaxation of the strain in the layers. Evidence for such a relaxation can be found in Ref. 21 where TEM studies of YBCO/PrBCO clearly indicate that the first several hundred Å of material are strained. Ongoing TEM studies realized by Bardal and Eibl on our samples, seem also to reveal such a transition although less marked than the one observed by Lia *et al.*<sup>21</sup> It is hard to see how strains

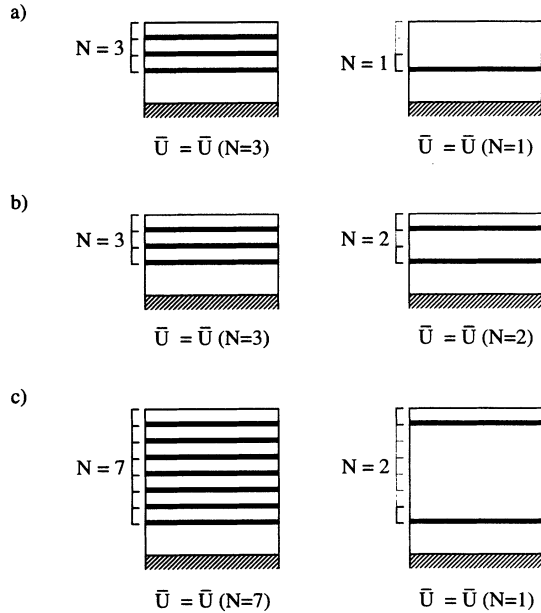


FIG. 7. Schematic diagrams of test samples measured to rule out possible dominant effects in activation energies due to changes in total sample thickness. (a) One compares a  $N=3$  DyBCO-( $Y_{0.45}Pr_{0.55}$ )BCO sample with a sample having the same total thickness but only one superconducting layer. (b) The central superconducting layer has now been removed in the test sample. (c) One compares here an  $N=7$  sample with a sample having identical total thickness but where only the top and bottom superconducting layers rest. Indicated below the diagrams are the corresponding measured activation energies.

can explain the linearity in  $\bar{U}(N)$  for the DyBCO-alloy series and the ratio of two between the  $N=1$  and  $N=2$  samples. Nevertheless, to make sure that what we do observe is not related to peculiar effects related to changes in, for instance, total sample thickness, we prepared a series of test samples shown in Fig. 7. We compared first a  $N=3$  DyBCO-( $Y_{0.45}Pr_{0.55}$ )BCO sample with a sample having the same total thickness but only one superconducting layer [illustrated in Fig. 7(a)]. Although a change in the onset of the transition was observed, the activation energy of the latter sample was within 10% identical to the  $N=1$  sample, as expected. Then we prepared a sample again identical to the  $N=3$  sample but whose central layer was “removed” [see Fig. 7(b)]. In this case we find that the activation energy of this sample corresponds, again within 10%, to the one of the  $N=2$  sample meaning that coupling is still present between the two superconducting layers. Finally we made a sample with the same total thickness as the  $N=7$  sample but where only the first and last superconducting layers are kept, see Fig. 7(c). In this last case the activation energy corresponds to the one of the  $N=1$  sample meaning that the coupling is negligible on such large distances. For this last sample the activation energy values are equal to those of the  $N=1$  sample to better than 10%, although for low resistances a change in slope is observed on the Arrhenius plot which would correspond to an even lower activation energy. From all these tests we did not find any correlation between total thickness and activation energies, comforting us in our interpretation of the data in terms of coupling.

## VI. NATURE OF THE COUPLING

Now we turn to the discussion of the coupling. We find for both alloys an effective coupling over at least a distance of 200 Å in the  $c$  direction, and which is not affected by a 9 T magnetic field. For the ( $Y_{0.6}Pr_{0.4}$ )BCO alloy we determined the coherence lengths from an estimate of  $H_{c2}$ . We find  $\xi_c(0) \approx 30$  Å and  $\xi_{ab}(0) \approx 60$  Å. This value of  $\xi_{ab}$  is close to the one obtained in Ref. 11. The reasonably “large”  $\xi_c(0)$  is certainly sufficient to explain coupling, due to the proximity effect, on characteristic distances of 100 Å, provided that the matching conditions at the interface are good enough. As mentioned earlier the magnetic coupling cannot be responsible for the observed effect. The main experimental evidence is that coupling is not observed when the alloy is replaced by insulating PrBCO, as shown in Fig. 6. Additionally, strong magnetic coupling occurs only when  $g_{10}d_i \ll 1$ ,<sup>22</sup> where  $g_{10} = (8\pi B / \sqrt{3}\phi_0)^{1/2}$  is the shortest reciprocal-lattice vector (for a triangular lattice) and  $d_i$  the separation distance between superconducting layers. For  $d_i = d - (Y_{1-x}Pr_x)BCO = 96$  Å,  $g_{10}d_i = 1$  for  $H \approx 1$  T. Above this field magnetic coupling should be negligible. Finally it has been shown<sup>23,24</sup> that magnetically coupled pancake vortices evaporate at the Kosterlitz-Thouless transition temperature  $T_{KT}$  meaning that the coupling energy is of the order of  $k_B T_{KT}$ . On the other hand, from this study one sees in Fig. 6 that the activation energies measured for the  $N=1$  DyBCO-alloy sam-

ples are between 200 and 400 K. This is much higher than the values of 20–30 K estimated for  $T_{KT}$ , confirming that magnetic coupling is too weak to play a substantial role in our particular system.

In the case of the  $(Y_{0.45}Pr_{0.55})BCO$  alloy, whose resistivity displays a semi-conducting-like behavior, the understanding of the nature of the coupling will require additional studies of the properties of the alloy itself. Since this material is close to a metal-insulator transition, the problem of a possible proximity superconductivity within the radius of localization has to be considered.

## VII. MAGNETIC-FIELD DEPENDENCE OF $\bar{U}$

As we mentioned in Sec. IV, the artificial structures we discuss here seem to be ideal to probe the effect of dimensionality on the properties of the vortex lattice. As a first step we measured in detail the magnetic-field dependence of the activation energies. For samples having a purely 2D vortex lattice, we found in numerous single layers and decoupled multilayers, that  $\bar{U}$  is proportional to  $\log_{10}B$ .<sup>3–6</sup> Such a dependence of the activation energy has also been recently measured in Mo/Ge multilayers.<sup>25</sup> The origin of this  $\log_{10}B$  dependence of the activation energy is still an open question at the moment. At least two ideas have been proposed to explain this particular field dependence. In Ref. 3 it was noticed that the theory of collective pinning of Feigel'man, Geshkenbein, and Larkin<sup>26</sup> implies that for a short translational correlation length  $R_c$ , the free energy to create a single vortex dislocation is finite, leading to an activation energy  $U$  proportional to  $-\alpha \log_{10}B + \beta$ . This interpretation was also adopted for explaining the behavior of Mo/Ge superlattices.<sup>25</sup> More recently, Jensen *et al.*<sup>27</sup> proposed that the  $\log_{10}B$  behavior may have a different origin, namely, the dominant contribution to the dissipation of thermally generated vortex-antivortex pairs. Here, the idea is that the field-induced vortices can screen the vortex of the thermally generated vortex-antivortex pair. In this case the mean vortex-antivortex distance is about  $a_0$ , the vortex lattice constant. With the energy between the vortex and the antivortex proportional to the logarithm of the separation and since  $a_0 \approx \sqrt{(\phi_0/B)}$ , with  $\phi_0$  the flux quantum, one gets  $U \approx -\alpha^* \log_{10}B + \beta^*$ .

Figure 8 is a plot of  $\bar{U}(H)$  for a  $N=15$  sample, top on a log-log scale, bottom on a log-lin scale. This sample is representative of the behavior of DyBCO- $(Y_{0.45}Pr_{0.55})BCO$  and DyBCO- $(Y_{0.6}Pr_{0.4})BCO$  samples. As one sees on the bottom part of the graph, we still observe the  $\log_{10}H$  behavior for fields below  $\approx 1$  T. However, for larger fields a clear deviation is apparent. In the present DyBCO-alloy samples having a 2D vortex lattice according to the activation energy measurements, deviations from the  $\log_{10}H$  behavior occur only at high fields ( $> 6$  T). In 3D vortex lattice samples and at high fields, the activation energy seems to turn into a power law,  $\bar{U} \approx H^{-\alpha}$  with  $\alpha=0.53$  for the particular sample shown in Fig. 8 (clearly because of the limited range of available high fields the precise determination of the power-law behavior is difficult). Depending on the samples we find values of  $\alpha$  ranging from 0.45 to 0.65, always close to 0.5.

We observe that the crossover field depends on the number of layers in the sample. Even if small fluctuations in the activation energies complicate the precise determination of the crossover field, one finds that the thicker the sample (or larger  $N$ ) the smaller the crossover field.

What could be the origin of this crossover? What we observe is a deviation from the  $\log_{10}H$  behavior at a field which depends on the total thickness. Above this characteristic field  $H^*$ , the measured activation energies are higher than what a continuation of the  $\log_{10}H$  dependence would give. The crossover field is certainly not the decoupling field, at which intralayer interactions dominate the interlayer interactions leading to an effective decoupling of the layers, since above  $H^*$  one does not at all recover the behavior of a single layer  $N=1$  sample. One possibility is that, at low field when the density of field-induced vortices remains low compared to thermally generated vortex-antivortex pairs, the dissipation is still dominated by a 2D-like behavior, while at high field, dissipation coming from the flux “lattice” becomes dominant. Another possibility is that the observed behavior is the result of the entanglement of the vortices, as discussed by Nelson<sup>28</sup> and Nelson and Seung.<sup>29</sup> The idea

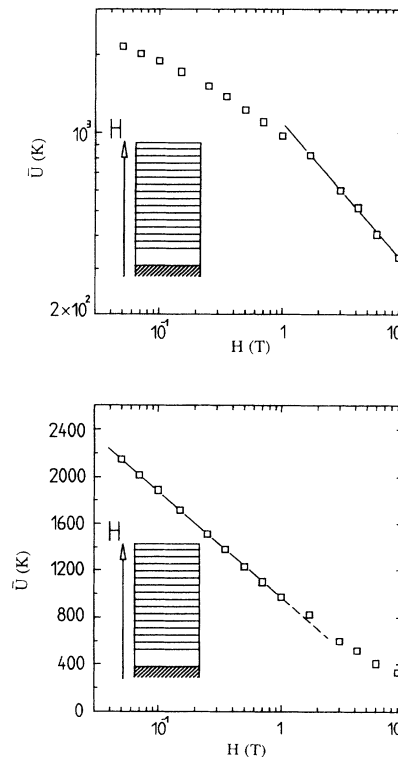


FIG. 8. Magnetic-field dependence of  $\bar{U}$  for the  $N=15$  sample of the DyBCO- $(Y_{0.45}Pr_{0.55})BCO$ . (Top) On a log-log plot, (Bottom) On a log-lin plot. As can be seen a deviation from the  $\log_{10}H$  behavior is observed above a characteristic magnetic field  $H^*$ . We find in the DyBCO-alloy series that  $H^*$  decreases as  $N$  increases. The insets show the structure of the  $N=15$  sample and the field configuration. The black lines are the 24-Å-thick DyBCO layers while the white regions are 230-, and 96-Å-thick  $(Y_{0.45}Pr_{0.55})BCO$ , for the buffer and the separation layers, respectively.

here is that the  $\log_{10}H$  behavior may not be only a characteristic of 2D systems, but more generally the characteristic of disentangled systems. As long as the vortices are rigid, entanglement is clearly impossible. For thin 3D samples and at low field the vortices are too far to entangle; as the field increases the distance between vortices decreases and entanglement becomes possible, resulting in an increase of the activation energy due to the flux line crossing energy.

The expression for the entanglement field is:<sup>28,29</sup>

$$H = \phi_0^3 (8\pi\mu_0 l_z k_B T \lambda_{ab}^2)^{-1} \left[ \frac{M_{ab}}{M_z} \right] \ln \left[ \frac{\lambda_{ab}}{\xi_{ab}} \right],$$

where  $l_z$  is the sample thickness,  $\lambda_{ab}$  is the in-plane penetration depth,  $\xi_{ab}$  is the in-plane coherence length,  $T$  is the temperature and  $M_{ab}$  and  $M_z$  are the effective mass. Setting  $\lambda_{ab} = 1400 \text{ \AA}$ ,  $\xi_{ab} = 12 \text{ \AA}$ ,  $T = 50 \text{ K}$ , and a mass ratio  $M_{ab}/M_z = 10^{-2}$  (this value is a rough estimate of the mass ratio), one gets  $H = 1200(l_z(\text{\AA}))^{-1}(\text{T})$ , where the entanglement field is in Tesla for  $l_z$  given in  $\text{\AA}$ . For the  $N = 15$  sample  $l_z = 1800 \text{ \AA}$  and the entanglement field  $\approx 0.7 \text{ T}$ , precisely in the range where we observe the crossover. The  $1/l_z$  dependence predicted by the above formula is consistent with the data, although large uncertainties arise in the determination of the crossover field. It is also interesting to notice that Vinokur *et al.* have predicted a  $B^{-0.5}$  behavior of the activation energy, as observed here at high fields, in the case of a very viscous flux lattice with large barriers associated with thermally activated plastic motion of the vortex structure.<sup>30</sup> They also note that such large barriers can arise due to entanglement of vortex lines.<sup>30</sup> Although very appealing, the explanation of our data in terms of entanglement will require additional confirmations to insure that other effects are not responsible for the observed behavior. Especially

the behavior of  $N < 3$  samples, for which deviations from the  $\log_{10}H$  behavior occur at high fields ( $> 6 \text{ T}$ ), needs further analysis to be understood within the concept of entanglement.

## VIII. CONCLUSIONS

In conclusion we have shown that a measure of the activation energies is a sensitive tool for studying coupling. We find that proximity coupling through  $(Y_{1-x}\text{Pr}_x)\text{BCO}$  is sufficient to induce coupled vortex motion. In  $24 \text{ \AA}$ - $\text{DyBCO}/96 \text{ \AA}$ - $(Y_{0.45}\text{Pr}_{0.55})\text{BCO}$  structures, it is found that three to four pancakes belonging to different DyBCO layers have a coupled motion. The correlation length  $L_c^*$  of these artificial materials is about  $300\text{--}500 \text{ \AA}$ . We find that the magnetic-field dependence of  $U$  changes going from the 2D vortex lattice where  $U$  is proportional to  $\log_{10}B$  to a more complicated behavior for 3D vortex lattice (large  $N$ ) where a crossover in field occurs. At low field the  $\log_{10}B$  behavior is preserved, at higher field the behavior seems to turn to power law with  $U \approx B^{-0.5}$ . The crossover is discussed in terms of possible entanglement of the vortices at high field.

## ACKNOWLEDGMENTS

We would like to thank R. Perez-Pinaya for his help in specific measurements, Dr. A. Bardal and Dr. O. Eibl for TEM investigations, Dr. A. Gupta for fruitful and stimulating discussions, and G. Bosch and A. Stettler for efficient technical support. This work was supported by the "Fonds National Suisse de la Recherche Scientifique." One of us (M.A.) would like to thank the Swedish Natural Science Research Council for financial support.

<sup>1</sup>See, for instance, the extensive review of G. Blatter, M. V. Feigel'man, V. B. Geshkenbein, A. I. Larkin, and V. M. Vinokur, *Rev. Mod. Phys.* (to be published).

<sup>2</sup>See, for instance, D. S. Fisher, M. P. A. Fisher, and D. A. Huse, *Phys. Rev. B* **43**, 130 (1991).

<sup>3</sup>O. Brunner, L. Antognazza, J.-M. Triscone, L. Miéville, and Ø. Fischer, *Phys. Rev. Lett.* **67**, 1354 (1991).

<sup>4</sup>Ø. Fischer, O. Brunner, L. Antognazza, L. Miéville, and J.-M. Triscone, *Phys. Scr. T* **42**, 46 (1992).

<sup>5</sup>Ø. Fischer, O. Brunner, L. Antognazza, J.-M. Triscone, L. Miéville, M. G. Karkut, P. van der Linden, and J. A. A. J. Perenboom, *Physica B* **177**, 87 (1992).

<sup>6</sup>O. Brunner, Ph.D. thesis, University of Geneva, 1993.

<sup>7</sup>A. I. Larkin and Yu. N. Ovchinnikov, *J. Low Temp. Phys.* **34**, 409 (1979).

<sup>8</sup>A. J. J. van Dalen, R. Griessen, H. G. Schnack, J.-M. Triscone, and Ø. Fischer, *J. Alloys Compounds* **195**, 447 (1993).

<sup>9</sup>J.-M. Triscone, P. Fivat, O. Brunner, R. Perez-Pinaya, M. Decroux, and Ø. Fischer, *Physica B* **194-196**, 2375 (1994).

<sup>10</sup>P. Fivat, J.-M. Triscone, and Ø. Fischer, *Supercond.* **7**, 181 (1994).

<sup>11</sup>E. Polturak, G. Koren, D. Cohen, E. Aharoni, and G. Deutscher, *Phys. Rev. Lett.* **67**, 3038 (1991).

<sup>12</sup>D. P. Norton, D. H. Lowndes, S. J. Pennycook, and J. D. Budai, *Phys. Rev. Lett.* **67**, 1358 (1991).

<sup>13</sup>Q. Li, C. Kwon, X. X. Xi, S. Bhattacharya, A. Walkenhorst, T. Venkatesan, S. J. Hagen, W. Jiang, and R. L. Greene, *Phys. Rev. Lett.* **69**, 2713 (1992).

<sup>14</sup>J. J. Neumeier and M. B. Maple, *Physica C* **191**, 158 (1992).

<sup>15</sup>J.-M. Triscone, Ø. Fischer, O. Brunner, L. Antognazza, A. D. Kent, and M. G. Karkut, *Phys. Rev. Lett.* **64**, 804 (1990).

<sup>16</sup>I. K. Schuller, *Phys. Rev. Lett.* **44**, 1597 (1980).

<sup>17</sup>O. Nakamura, E. Fullerton, J. Guimpel, and I. K. Schuller, *Appl. Phys. Lett.* **60**, 120 (1992).

<sup>18</sup>P. Fivat, I. Maggio-Aprile, J.-M. Triscone, and Ø. Fischer (unpublished).

<sup>19</sup>T. T. M. Palstra, B. Battlogg, R. B. Van Dover, L. F. Schneemeyer, and J. V. Waszczak, *Phys. Rev. B* **41**, 6621 (1990).

<sup>20</sup>J.-M. Triscone, P. Fivat, O. Brunner, R. Perez-Pinaya, M. Decroux, and Ø. Fischer, *J. Alloys Compounds* **195**, 181 (1993).

<sup>21</sup>C. L. Lia, H. Soltner, G. Jakob, T. Hahn, H. Adrian, and K. Urban, *Physica C* **210**, 1 (1993).

<sup>22</sup>J. W. Ekin, B. Serin, and J. R. Clem, *Phys. Rev. B* **9**, 912 (1974).

<sup>23</sup>L. N. Bulaevskii, S. V. Meshkov, and D. Feinberg, *Phys. Rev.*

- B **43**, 3728 (1991).
- <sup>24</sup>J. R. Clem, *Phys. Rev. B* **43**, 7837 (1991).
- <sup>25</sup>W. R. White, A. Kapitulnik, and M. R. Beasley, *Phys. Rev. Lett.* **70**, 670 (1993).
- <sup>26</sup>M. V. Feigel'man, V. B. Geshkenbein, and A. I. Larkin, *Physica C* **167**, 177 (1990).
- <sup>27</sup>H. J. Jensen, P. Minnhagen, E. Sonin, and H. Weber, *Europhys. Lett.* **20**, 463 (1992).
- <sup>28</sup>D. R. Nelson, *Phys. Rev. Lett.* **60**, 1973 (1988).
- <sup>29</sup>D. R. Nelson and H. S. Seung, *Phys. Rev. B* **39**, 9153 (1989).
- <sup>30</sup>V. M. Vinokur, M. V. Feigel'man, V. B. Geshkenbein, and A. I. Larkin, *Phys. Rev. Lett.* **65**, 259 (1990).